Geophysical Research Letters

RESEARCH LETTER
10.1029/2021GL096544

Key Points:

- Tropical-cyclone (T-C) convective-scale turbulence is not isotropic/homogeneous, thus possessing different predictability properties from classical turbulence
- T-C error-energy spectra show distinct characteristics with a steeper power law in the radial direction than that in the azimuthal direction
- T-C error energy spectral growth is more rapid for the azimuthal wavenumbers than for radial wavenumbers, reaching saturation after ~18 hr

Supporting Information:

Supporting Information may be found in the online version of this article.

Correspondence to:

C. Kieu,
ckieu@indiana.edu

Citation:

Kieu, C., & Rotunno, R. (2022). Characteristics of tropical-cyclone turbulence and intensity predictability. *Geophysical Research Letters*, *49*, e2021GL096544. https://doi.org/10.1029/2021GL096544

Received 13 OCT 2021
Accepted 9 MAR 2022

Author Contributions:

Conceptualization: Chanh Kieu, Richard Rotunno
Formal analysis: Chanh Kieu, Richard Rotunno
Funding acquisition: Chanh Kieu
Investigation: Chanh Kieu
Methodology: Chanh Kieu, Richard Rotunno
Project Administration: Chanh Kieu, Richard Rotunno
Supervision: Richard Rotunno
Validation: Chanh Kieu, Richard Rotunno
Visualization: Chanh Kieu, Richard Rotunno
Writing – original draft: Chanh Kieu, Richard Rotunno

Characteristics of Tropical-Cyclone Turbulence and Intensity Predictability

Chanh Kieu[1,2] and Richard Rotunno[3]

[1]Department of Earth and Atmospheric Science, Indiana University, Bloomington, IN, USA, [2]Now at NOAA Geophysical Fluid Dynamics Laboratory, Princeton University, Princeton, NJ, USA, [3]National Center for Atmospheric Research, Boulder, CO, USA

Abstract This study examines the characteristics of tropical-cyclone (T-C) turbulence and its related predictability implications. Using the Fourier-Bessel spectral decomposition for convection-permitting simulations, it is shown that T-C turbulence possesses different spectral properties in the azimuthal and radial directions, with a steeper power law in the radial-wavenumber than that in the azimuthal-wavenumber direction. This spectral difference between the azimuthal and radial directions prevents one from using a single wavenumber to interpret T-C intensity predictability as for classical homogeneous isotropic turbulence. Analyses of spectral error growth for a high-wavenumber perturbation further confirm that the spectral growth is more rapid for high azimuthal wavenumbers than for the radial wavenumbers, reaching saturation after ~9 hr and ~18 hr for the azimuthal and radial directions, respectively. This result highlights the key difficulty in quantifying T-C intensity predictability based on spectral upscale error growth for future applications.

Plain Language Summary This study examines the characteristics of tropical cyclone (T-C) turbulence and related predictability implications. We show that T-C turbulence possesses different spectral properties in the azimuthal and radial directions. This spectral difference between the azimuthal and radial directions prevents one from using a single wavenumber to interpret T-C intensity predictability as for classical homogeneous isotropic turbulence. Our analyses of spectral kinetic energy error growth at the quasi-stationary stage reveal that the spectral growth is more rapid for azimuthal wavenumbers, reaching saturation after ~9 hr as compared to ~18 hr for the radial direction. This study highlights the difficulty in quantifying T-C intensity predictability based on spectral upscale error growth for practical applications.

1. Introduction

The tropical cyclone (TC) is a multiscale nonlinear system in which any small-scale perturbation could amplify and progressively influence larger scales, resulting in T-C intensity variability. This type of upscale-error growth, termed the "real butterfly effect" (Palmer et al., 2014), exists in various fluid-flow systems and determines their intrinsic predictability. Unlike deterministic systems whose predictability is governed by Lyapunov exponents and attractor invariants (e.g., Alligood et al., 2000; Aurell et al., 1996; Boffetta et al., 1998; Goldhirsch et al., 1987; Lorenz, 1963; Palmer, 1993), quantifying predictability related to upscale growth in multi-scale systems requires knowledge of the system's statistically stationary turbulence. As extensively examined in previous studies (e.g., Kraichnan, 1967; Leith & Kraichnan, 1972; Lorenz, 1969; Palmer et al., 2014; Rotunno & Snyder, 2007; Schneider & Griffies, 1999), such a stationary background contains key characteristics of turbulence flows and plays a fundamental role in atmospheric-predictability research.

Given a background energy spectrum for a turbulent system, predictability is often defined as the time interval beyond which a forecast probability distribution of a system state variable becomes indistinguishable from its climatological probability distribution (DelSole, 2004; DelSole & Tippett, 2007; Lorenz, 1969; Schneider & Griffies, 1999; Shukla, 1981). From this formal definition, it is apparent that the predictability limit is not a universal metric but depends on the variable and its climatology. For example, the same variable can have a different predictability if a different time scale or observation is used to construct its climatology. Using a two-dimensional (2D) model of statistically stationary, isotropic homogeneous turbulence and kinetic energy as the metric of error growth, Lorenz (1969, hereinafter L69) established the important result that fully developed 2D turbulence with a power-law energy spectrum $\Gamma(k) \sim k^n$ implies limited predictability for $n = -5/3$, while $n \leq -3$ implies unlimited predictability.

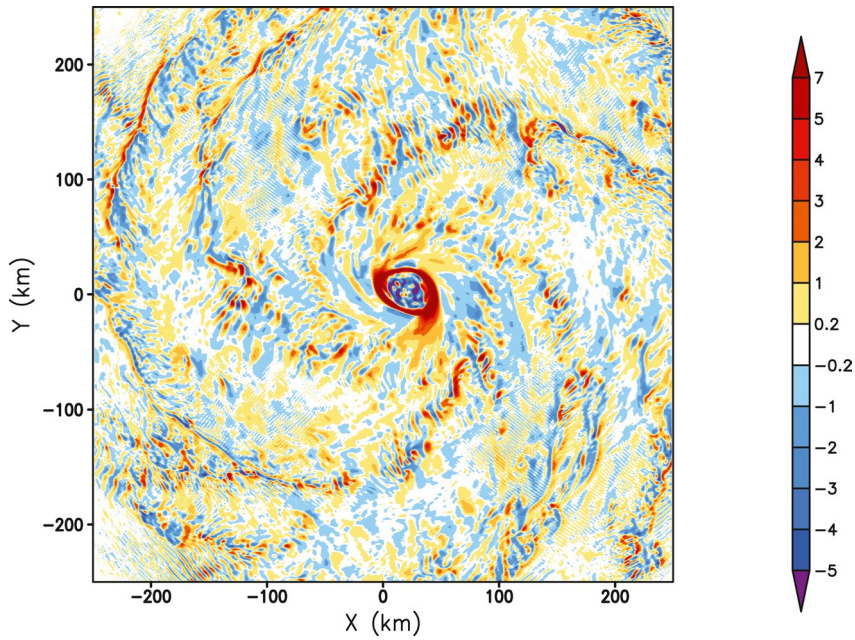

Figure 1. A snapshot of the horizontal distribution of the vertical component of vorticity perturbation (unit 10^{-4} s^{-1}) valid at $t = 90$ hr. Here, the perturbation is computed as a difference between the instantaneous output at $t = 90$ hr and the average obtained during the quasi-stationary stage ($t = 72 - 120$ hr) of the Hurricane Weather Research and Forecasting simulation.

How to apply Lorenz's predictability framework to T-C intensity is, however, a nontrivial question for several reasons. First, the evolution of a TC is by definition time-dependent. Unlike the classical predictability framework in which a fully developed stationary state of turbulence is well-defined, TCs evolve with time, starting first as a tropical depression followed by subsequent development into a mature TC at peak intensity and eventual dissipation. While TCs may possess a stable equilibrium regime during which the quasi-stationary property applies (Kieu, 2015; Kieu and Wang, 2017; Hakim, 2011, 2013; Rotunno & Emanuel, 1987), in practice a T-C intensity forecast requires predicting T-C intensity from its very early stage to its end. The question of practical T-C intensity predictability is therefore fundamentally different from the traditional framework for intrinsic predictability in which a statistically stationary energy spectrum is required. That is, T-C intrinsic intensity predictability cannot be defined for the entire T-C evolution, simply because it is meaningless to have a climatological distribution that is a function of both forecast lead-time and time. The T-C intensity problem in this sense can be pictured as a Lorenz (1963)-type model with its butterfly-wing attractor expanding over time; for this case, predictability is not well-defined.

Second, T-C dynamics are not homogeneous and isotropic, even at the quasi-stationary stage. Unlike homogenous isotropic turbulence in which all points and directions in space are indistinguishable, TCs possess a unique center in physical space where the dynamics and thermodynamics are different from elsewhere. Furthermore, T-C turbulence possesses coherent structures ranging from convective-to meso-scale, as illustrated in Figure 1. These coherent structures prevent one from applying the traditional spectral analysis for homogenous isotropic turbulence to study T-C error growth. Hence, the question of estimating intrinsic T-C-intensity predictability is still open, despite the strong suggestion of limited practical intensity predictability from real-time forecasts and numerical simulations (Kieu and Moon, 2016; Kieu et al., 2018; Emanuel & Zhang, 2016; Hakim, 2011, 2013; Judt et al., 2015).

Given the above issues, which are very specific to T-C intensity, the objectives of this study are to (a) present a system-appropriate definition of the T-C turbulence spectrum so that the scales of T-C turbulence can be quantified, and (b) propose estimates of intrinsic T-C intensity predictability within the present multiscale spectral analyses.

2. Methodology

2.1. Experiment Design

In this study, a cloud-resolving idealized configuration of the Hurricane Weather Research and Forecasting (HWRF) model was used to examine T-C turbulence. Similar to the setting used in Kieu et al. (2018, hereinafter K18), the HWRF simulations were carried out with a nested resolution of ~8.1, 2.7 km, and 900 m to best capture the convective-scale turbulence (see Section S1 of the Supporting Information S1 for more details of all model configurations used in this study).

With this HWRF idealized configuration and a control simulation that can capture the simulated T-C quasi-stationary stage as in K18, an external axisymmetric error is then added to the model vortex at the mature stage to examine the evolution and related upscale growth of the error. Here, we give the initial error $v'(r,0)$ as

$$v'(r, t=0) = A\sin(k_0 r), \tag{1}$$

where A is the amplitude of the initial perturbation, r is the radius from the vortex center, and k_0 is the prescribed wavenumber. For this study, the initial perturbation 1 is generated for the horizontal wind field (u', v') with $A = 10^{-3}$ m s^{-1} and is added every 6 hr during the mature stage of the model vortex, resulting in a total of 12 perturbed integrations between 72 and 120 hr. Perturbing other variables such as temperature or relative humidity gave the same results and will not be presented here.

With the main objective of studying how high-radial-wavenumber noise could grow upscale given T-C background dynamics, k_0 is chosen to be $(3\Delta x)^{-1}$ in all experiments, which is the highest wavenumber that can be resolved on the HWRF model grid Δx. For high wavenumbers k_0, we note that the Bessel function can be approximated as a sinusoidal function and so the initial structure 1 ensures the spike at $k = k_0$ in the spectral space as expected. Note also that due to the nature of the regional HWRF model with a rectangular domain and wave-radiative lateral boundary conditions, only initial errors with radial dependence, as given in Equation 1, are used in our spectral error-growth analysis. Constructing initial errors that vary along the azimuthal direction is not feasible due to the domain grid structure and the HWRF finite-difference schemes. This issue is especially apparent in the eye region, where the number of model grid points is always limited around the center of the model vortex.

2.2. Spectral Analyses

Given the nearly circular homogeneity of the TC for each radius, we employ in this study a combination of Fourier and Bessel decompositions to analyze T-C turbulence in polar coordinates. Specifically, the Fourier transform is first applied to any variable $f(r,\theta)$ along the azimuthal direction at each radius in the polar coordinates (r,θ) as

$$f_m(r) = \int_0^{2\pi} f(r,\theta) e^{-i2\pi m\theta} d\theta. \tag{2}$$

The Fourier components $f_m(r)$ are then decomposed by the Hankel transform based on Bessel functions in the radial direction as:

$$F_m(k) \equiv \int_0^{\infty} f_m(r) J_m(kr) r dr, \tag{3}$$

where $J_m(r)$ is the Bessel function of the first kind of order m which forms an orthogonal basis through the relation,

$$\int_0^{\infty} J_m(pr) J_m(qr) r dr = \frac{\delta(p-q)}{p},\ \forall (p,q) > 0. \tag{4}$$

Technically, this decomposition sequence is equivalent to the Fourier-Bessel transform, which is a natural extension of the 2D Fourier transform (Piessens, 2010). In fact, it can be shown that a particular class of the Fourier-Bessel transform with the zeroth-order Bessel function is equivalent to the 2D Fourier transform of circularly

symmetric functions (see, e.g., Piessens, 2010). In all Bessel decompositions presented in this study, the discrete version of the Hankel transform 3 developed by Leutenegger (2007) is applied for a finite domain range [0, R], where the maximum radius R is set to be 250 km (roughly the size of the innermost domain).

Because of the lack of homogeneity of T-C turbulence, a direct 2D Fourier-transform of (u', v', w') would not render a correct spectral energy interpretation. However, for each radius, T-C turbulence can be well approximated as a statistically homogenous flow due to the circular symmetry of TCs in a statistically stationary state. As such, one can apply the Fourier transform along the azimuthal direction to obtain the following kinetic energy spectral density at each radius

$$e(m,r) = \frac{\overline{u_m(r)u_m^*(r)} + \overline{v(r)v_m^*(r)} + \overline{w_m(r)w_m^*(r)}}{2\pi}, \tag{5}$$

where $u_m(r), v_m(r), w_m(r)$ are the Fourier coefficients of the wind perturbation components in cylindrical coordinates (u', v', w') as defined in Equation 2, and the bar denotes the time average over the quasi-stationary stages. The energy spectral density is well defined on a finite domain [0, R], because Parseval's theorem ensures that the total energy $E(r)$ at each radius r satisfies:

$$E(r) = \int_0^\infty e(m,r)dm = \frac{1}{2}\int_0^{2\pi} \left[\overline{u'^2(r,\theta)} + \overline{v'^2(r,\theta)} + \overline{w'^2(r,\theta)}\right] d\theta. \tag{6}$$

Given the Fourier coefficients $u_m(r), v_m(r), w_m(r)$, the Hankel transform of these coefficients using Bessel functions gives $\hat{u}_m(k), \hat{v}_m(k), \hat{w}_m(k)$ according to Equation 3. Note that the Hankel transform also has a Parseval's identity of the form.

$$\int_0^\infty |\hat{u}_m(k)|^2 k dk = \int_0^\infty |u_m(r)|^2 r dr\,. \tag{7}$$

One can therefore define the energy spectral density in $k-m$ space as

$$\hat{E}(k,m) = \overline{|\hat{u}_m(k)|^2} + \overline{|\hat{v}_m(k)|^2} + \overline{|\hat{w}_m(k)|^2}; \tag{8}$$

The integration of Equation 8 over both the k and m directions gives the total error kinetic energy (TKE) as expected (see in Supporting Information S1)

$$TKE = \int_0^\infty dm \int_0^\infty \hat{E}(k,m)kdk \tag{9}$$

Thus $\hat{E}(k,m)$ can be properly interpreted as an energy spectral density of T-C turbulence (see the Supporting Information S1 for the derivation).

Several remarks are in order here on the above spectral decompositions when applying them to T-C turbulence. First, unlike homogeneous isotropic turbulence in which there is circular (or spherical in 3D) symmetry of the energy spectrum in the Cartesian wavenumber space (i.e., the 2D energy spectrum can be considered a function of the single wavenumber $\kappa \equiv |\mathbf{k}| = \sqrt{k^2+m^2}$), the energy spectra of T-C turbulence must be characterized by two separate wavenumbers (k,m) separately as expressed in Equation 9. This is because the inhomogeneity of T-C turbulence essentially prevents one from using a single wavenumber to characterize the entire energy spectral density $\hat{E}(k,m)$. Thus, one must examine the spectral error growth and saturation for both directions k and m. This inhomogeneity of T-C turbulence is in fact reflected in previous studies, which have employed different approaches in examining T-C intensity predictability. For example, Judt et al. (2015) carried out the radially averaged spectral analyses in the azimuthal direction, whereas Vonich and Hakim (2018) performed spectral analyses along the radial direction of flight legs. Note however that the observational analyses in Vonich and Hakim (2018) or simulations of a real TC in Judt et al. (2015) contain a mix of various stages of TC development that do not generally satisfy the assumption of statistically stationary turbulence for spectral analyses. Also, T-C-turbulence spectra differ from those of the 2D isotropic homogeneous turbulence examined in, for example, Lorenz (1969), Leith and Kraichnan (1972), Mathieu (2000), or Rotunno and Snyder (2007). Therefore,

any interpretation of intensity predictability from T-C energy spectral density based on analogies with classical turbulence must be viewed with caution.

Second, the Fourier-Bessel spectral decomposition is applied only to the 2-D wind field at $z = 950$ hPa where the maximum wind closely represents T-C intensity. This application of the Fourier-Bessel transform at one specific level is motivated by the near circular homogeneity of T-C turbulence at each atmospheric level. In the vertical direction, the nature of the 3-D distribution of T-C turbulence is unknown, because of the baroclinic T-C structure in addition to its lack of isotropy. As such, the present study will be restricted to a single level at which the simulated turbulence is most intense.

3. Results

To illustrate first the properties of T-C turbulence, Figure 1 shows the structure of the relative-vorticity perturbation, which is obtained from the 900-m resolution domain during the mature stage (80–120 hr into the integration). One notices in Figure 1 a range of features whose spatial scales are from $\mathcal{O}\left(10^3\right) - \mathcal{O}\left(10^5\right)$ m, with dominant clusters organized at the convective scale within the strong rotational background. Moreover, these convective-scale features possess a well-defined center with the largest amplitude in the eyewall region, regardless of model variables and physical parameterization (not shown). The existence of such a center in T-C turbulence is also true for any snapshot taken during the maximum-intensity equilibrium, highlighting the key difference between T-C turbulence on a vortex background and classical homogeneous turbulence on a constant-mean-flow background.

Physically, the existence of such organized rings of turbulence as seen in Figure 1 is due to the T-C dynamics, which has strong vertical motion in the eyewall/rainband regions that distinguish a T-C vortex from pure 2D vortices. Note that if very high resolution is used to capture much finer spatial scales ($< \mathcal{O}(1)$ m) such as in large-eddy simulations (LES), then all turbulence at these fine scales should behave as classical turbulence superimposed on an approximate constant background flow, even if the turbulence is embedded within a T-C vortex (see, e.g., Worsnop et al., 2017). The 900-m horizontal and ~50-m vertical resolutions used in this study are apparently too coarse for examining such fine-scale turbulence. However, we observe that it is the organized convective-scale turbulence that is most relevant to T-C intensity variability, which is normally defined as a 1-min average of the maximum surface wind, instead of very small spatial and short temporal scales. This justifies our interpretation of convective-scale structures as T-C turbulence, instead of microscale turbulence $\mathcal{O}\left(10^{-3} - 10^{0}\right)$ m on a constant-flow background. This point is worth mentioning here, because it is central for defining the variability that is most relevant for T-C intensity. Given the distinct T-C convective-scale features as seen in Figure 1, the classical models for isotropic homogeneous turbulence cannot therefore be applied to T-C turbulence.

Given the properties of T-C turbulence, we next examine the saturated-error energy spectrum associated with the T-C convective-scale structures. This spectrum provides the predictability limit as a function of scale for time-evolving error-energy spectra, which is essential for determining TC-intensity predictability. Figure 2 shows the error kinetic energy (EKE) spectrum $e(r, m)$ for the fully developed T-C turbulence, where the Fourier azimuthal wavenumber m is defined in Equation 2. Here the azimuthal spectrum is area-averaged as in Judt et al., [2015; See their Equation 1] to remove the dependence of the background rotational flow with radius that produces different spectra for different radii. Despite the T-C background dynamics, one notices that the EKE spectra possesses a roughly "−5/3" power law for high azimuthal wavenumbers ($m \in [50 - 100]$) and an approximately "−3" power law for lower wavenumbers $m \in [5 - 20]$, as for the spectra of 3D and 2D homogeneous turbulence, respectively. This result is somewhat anticipated because T-C turbulence along the azimuthal direction can be approximately homogeneous.

If one applies the classical predictability interpretation as in Lorenz (1969)'s study that all power spectra with slopes less than −3 imply indefinite predictability, it is tempting to infer that the EKE spectral density obtained seen in Figure 2 indicates that T-C intensity is more predictable for the low azimuthal wavenumbers than that of high wavenumber m. However, this interpretation must be viewed with caution because it is based entirely on an isotropic homogeneous turbulence model with statistical closures that may not be applied for T-C turbulence. In addition, the restriction of the spectral decomposition for TC turbulence on each separate radius prevents one from having a full picture of the error-energy distribution in all directions, thus preventing us from applying Lorenz (1969)'s predictability interpretation for T-C intensity simply from the EKE spectrum in Figure 2a.

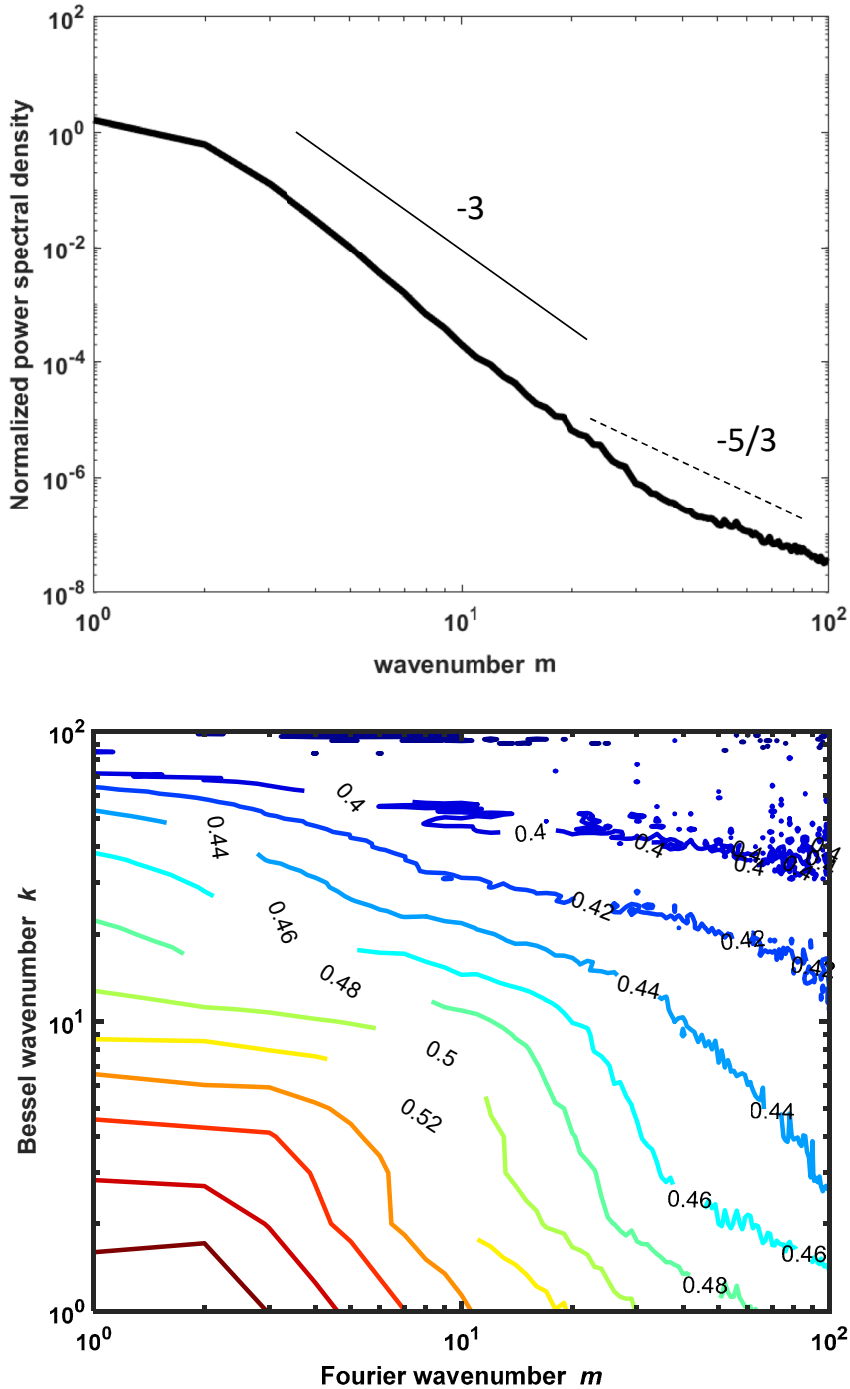

Figure 2. (a) Stationary error kinetic energy spectra as a function of the Fourier azimuthal wavenumber m i.e., area-averaged from 0 to 250 km; (b) the 2D spectral decomposition coefficient $\hat{E}(k,m)$ of error energy using Fourier-Bessel transform as given by Equation 8. This stationary background spectrum is constructed from the mature stage of the Hurricane Weather Research and Forecasting simulation during $t = 84 - 120$ hr. Note that all spectra are normalized by a factor $N \equiv \max_{k,m}|\hat{E}(k,m)|$ such that the maximum spectra are scaled to 1, and the Fourier-Bessel wavenumbers (k,m) are both nondimensional as defined in Equations 2 and 3.

To provide further insight into the EKE spectral distribution in the radial direction, Figure 2b shows the spectral density $\hat{E}(k,m)$ obtained from Equation 8. Unlike homogeneous isotropic turbulence, the 2D spectral density of T-C turbulence does not generally possess circular symmetry in wavenumber space, except for the low

wavenumbers. The difference in the EKE spectra between the azimuthal and radial direction is most clear if one compares the projection of $\hat{E}(k, m)$ along the k direction for low m wavenumbers or the m direction for low k wavenumbers, which have very different power laws for high wavenumbers in the spectral space (k, m) (cf. Figure 3).

Physically, the spectral difference between the m and k directions can be attributed to the fact that T-C turbulence tends to "lump" together at the radius of maximum wind (RMW) or the rainband locations in the radial direction instead of homogeneously spreading out in physical space (cf. Figure 1). Even along the azimuthal direction, we note that convective-scale turbulence tends to favor the wavenumbers $m = 1$ and 2 asymmetries presumably due to eyewall-stability dynamics (see, e.g., Schubert et al., 2007) or upscale cascade. This dominance of low wavenumbers in the azimuthal direction is especially clear if the environment has vertical wind shear or the β-effect is allowed, which will produce a distinctive wavenumber $m = 1$ asymmetry (e.g., Yang et al., 2007; Yu et al., 2015; Zhang & Kieu, 2005). From this perspective, the EKE decomposition shown in Figure 2b illustrates the fundamental difference between T-C turbulence and classical turbulence.

With the error-energy background shown in Figure 2, we now examine how an initial small-scale error grows in this T-C-background environment. This is a central step in quantifying T-C intensity predictability because the timescale for an initial error to grow and approach its stationary background spectrum in a multiscale system is defined as the predictability limit. This definition of predictability limit is general for any multiscale turbulent fluid flow that has no multiple equilibria, and it has been applied over a wide range of scales and problems (see, e.g., L69; Aurell et al., 1996, 1997; Boffetta et al., 1998; Durran et al., 2013; Judt, 2018; Leith, 1971; Métais & Lesieur, 1986; Rotunno & Snyder, 2007; Tribbia & Baumhefner, 2004). Thus, the upscale growth of an initial error in a given background spectrum is an inherent property of multiscale systems, which is more relevant to the predictability limit than the simple linear error growth in a low-order model (e.g., Palmer et al., 2014; Vallis, 2017).

Figure 3 shows the evolution of EKE spectrum in the (k, m) spectral space for an initial radial wavenumber given by Equation 1. One notices a few interesting features from the sequence of error-energy growth. First, the spectral-error evolution does not display a similar growth in the k and m directions in spectral space. Indeed, the most rapid error growth displays a consistent spectral error growth first at all azimuthal scales with $m > 50$ (the error spectrum is already near saturation after $\sim$ 3 hr for larger m), reaching saturation after 9 hr without any apparent upscale growth (Figure 3c). In contrast, the spectral-error growth in the k direction shows a slower error saturation, starting first with high- k wavenumbers and then the smaller wavenumbers (Figure 3d). If one applies the classical definition of predictability as the time interval during which an initial error would grow and occupy, for example, 95% of the total background spectrum, it is apparent from Figure 3 that the m wavenumbers, which characterize T-C turbulence in the azimuthal direction, suggest a predictability limit of <18 hr while the k wavenumbers indicate a longer range of predictability.

Second, unlike classical 3D turbulence models in which an initial error grows upscale from the smallest spatial scale to a larger scale progressively, one notices in Figure 3 that the spectrum tends to progress differently for different wavenumbers, with a faster growth rate for the high wavenumbers in both the k and m directions. Physically, the more rapid growth of the EKE spectrum in the high-wavenumber regime reflects the fact that any initial high-wavenumber perturbation tends to immediately break into convective-scale perturbations around the TC center. Indeed, a parallel analysis of error growth in physical space (Figure 4) confirms the breaking of the initial noise rings given by Equation 1 right after the noise is introduced into the simulation. These convective-scale perturbations subsequently evolve and are accumulated at the RMW and/or spiral band locations where convective activity is most vigorous. Because the outer-core bands are much-less organized as compared to the inner-core region (Figure 4), the concentration of outer-core error energy in the high-wavenumber regime is expected.

We note that the behavior of the spectral growth for the very high wavenumber regimes (k or $m \geq 90$), which appear to be the last to saturate (Figures 3c–f), is an elusive feature. While the difference between the T-C and the classical homogeneous turbulence may account for such a different spectral growth, the high-wavenumber regimes are also strongly affected by model resolution on a gridded domain, which prevents one from drawing any significant conclusion. Regardless of this uncertainty, the strong rotational vortex background of T-C dynamics with unique eyewall and spiral-band structure apparently provides different properties of error growth for T-C turbulence from that of classical turbulence models.

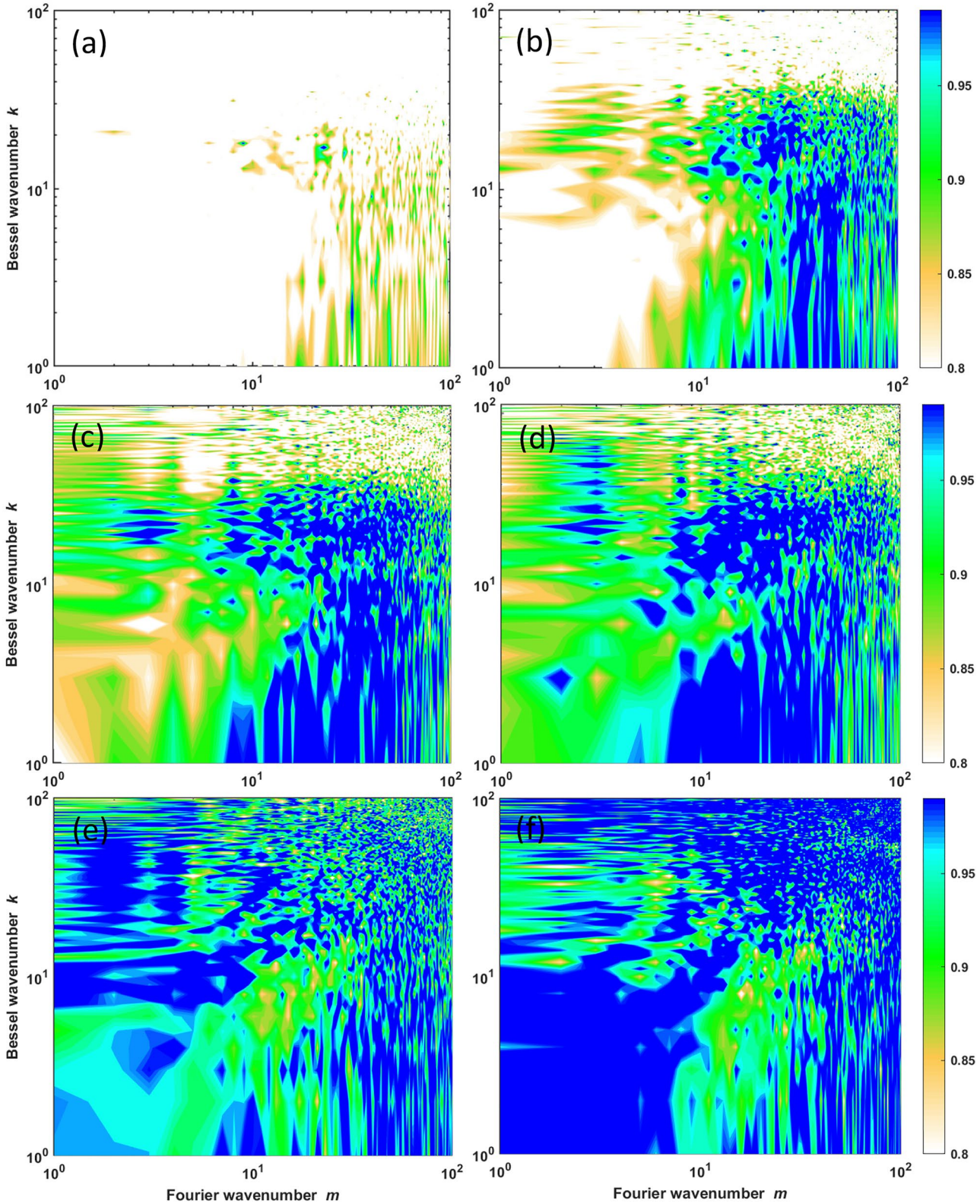

Figure 3. The evolution of the normalized 2D spectra $\hat{E}(k, m)$ of the error kinetic energy (shaded) relative to the stationary background spectrum shown in Figure 2b. These evolving spectra are valid at (a and b) 10 and 30 min, (c–f) 3, 9, 15, and 18 hr after the high-wavenumber noise is added to the model vortex during the quasi-stationary stage. Both wavenumbers (k, m) are nondimensional as defined in Equations 2 and 3.

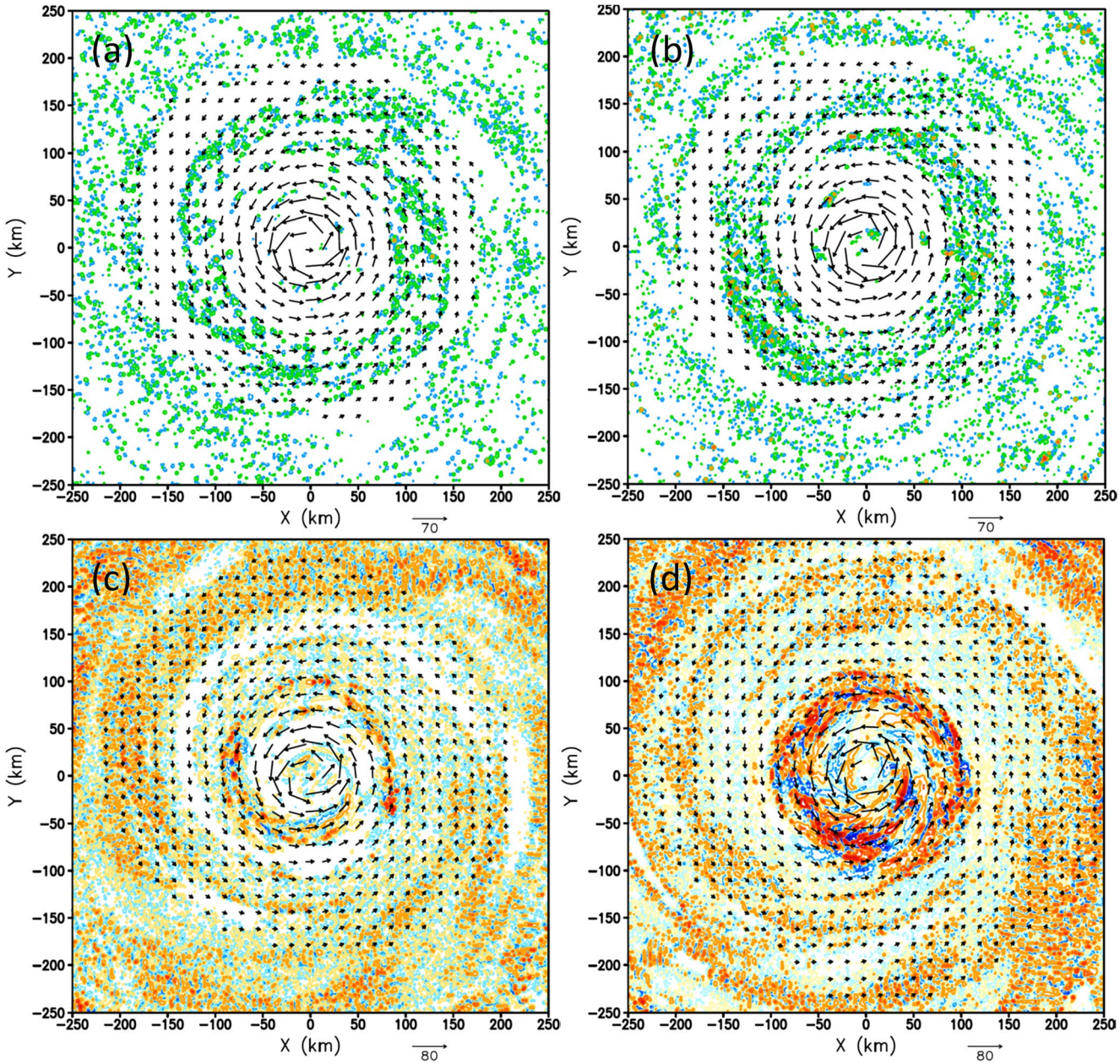

Figure 4. The two-dimensional evolution of wind speed (contours) in the physical space when an initial high-wavenumber noise given by Equation 1 is injected into the model quasi-stationary stage ($72 - 120\,hr$) for (a and b) 10 and 30 min at intervals of $\pm 0.01 \pm 0.05, \pm 0.1, \pm 0.5, \pm 1\ ms^{-1}$, and (c and d) 3 and 9 hr at intervals of $\pm 0.1, \pm 0.5, \pm 1, \pm 2, \pm 3\ ms^{-1}$ after the initial noise is added. Superimposed are the corresponding horizontal flow (vectors) at the 950-hPa level.

4. Concluding Remarks

In this study, the error-energy spectrum of fully developed turbulence and related error growth in a simulated TC were examined. Using the Fourier-Bessel transform for high-resolution HWRF model simulations, it was shown that T-C convective-scale turbulence does not possess properties typical of isotropic homogeneous turbulence. Instead, T-C turbulence tends to organize strongly around the eyewall and spiral-band regions, with a well-defined center similar to the background vortex. These organized patterns of T-C convective-scale turbulence are persistent during the mature stage of the model-simulated T-C vortex, regardless of model configurations, physical parametrizations, or variables used to quantify T-C turbulence.

From a practical standpoint, the consequence of such distinctive patterns of T-C turbulence is significant, because it suggests that the classical interpretation of homogenous turbulence likely does not be apply to T-C intensity predictability. That is, it is not sufficient to use a single wavenumber to represent the spectrum of T-C error energy in the two-dimensional plane. Instead, one must consider the azimuthal and the radial directions jointly to properly define the error-energy spectral density. Our analyses show that area-averaged TC turbulence can be approximately treated as homogeneous only in the azimuthal direction, which has an energy spectrum with a "~ -3" slope for low-m and "$\sim -5/3$" for high-m wavenumbers. Along the radial direction, the error energy spectrum does not appear to possess the classical power law for any range of k wavenumbers. This result supports our finding that T-C intensity predictability cannot be uniformly defined in both the azimuthal and radial directions.

Further analyses of the spectral growth of T-C EKE revealed several noteworthy features that are very specific to T-C turbulence. Looking along the azimuthal-wavenumber direction, it is found that the EKE spectrum grows most rapidly for the high m, reaching saturation after just ~3 hr. For the lower m, the error-energy growth exhibits a slower growth rate, approaching saturation after ~9 hr. In contrast, the error-energy growth along the radial direction displays a significantly slower rate, reaching saturation after ~18 hr. Note that this range of 9–18 hr is considerably shorter than the previous estimation of T-C intensity predictability, as it is applied only to the quasi-stationary stage of T-C development. These results highlight the difficulty in applying the traditional predictability interpretation as obtained from isotropic homogeneous turbulence to T-C turbulence. That is, one should not simply use any single direction to draw conclusions on T-C intensity predictability from spectral analyses as done for classical isotropic homogeneous turbulence.

We should emphasize that any intensity predictability implication derived from the simulations of T-C turbulence must be viewed with caution. This is because our approach of using the Fourier-Bessel transform in the 2D plane at each level is just one among several possible approaches. One could, for example, choose the radial direction of wind profile for energy spectra as in Vonich and Hakim (2018) or use an axisymmetric model for spectral analyses along the radial-vertical directions (Hakim, 2013), which could provide different estimation for T-C intensity predictability. Further development using the spectral approach requires a derivation of an error-energy spectral equation that can account for how the error energy grows upscale in radial-azimuthal wavenumber space. Such an equation does not exist currently but will be needed before one can understand the intrinsic predictability limit of T-C intensity.

Data Availability Statement

All HWRF simulations in this study employ an input sounding taken from Jordan (1958). Model output data used to generate spectral analyses in this study is available at: https://doi.org/10.13140/RG.2.2.18423.09126.

Acknowledgments
This research was partially supported by the Office of Naval Research (ONR) Young Investigator Award (N000141812588) and ONR/Tropical Cyclone Rapid Intensification program (N000142012411). The first author also wishes to thank the NCAR/Advanced Study Program visiting program for their summer support and hospitality during the preparation of this work. We also thank Falko Judt and two anonymous reviewers for their helpful comments and suggestions. Richard Rotunno is supported by the National Center for Atmospheric Research, which is a major facility sponsored by the National Science Foundation under cooperative agreement 1852977.

References

Alligood, K. T., Sauer, T., & Yorke, J. A. (2000). *Chaos: An introduction to dynamical system* (p. 603). Springer Publisher.

Aurell, E., Boffetta, G., Crisanti, A., Paladin, G., & Vulpiani, A. (1996). Growth of non-infinitesimal perturbations in turbulence. *Physical Review Letters*, *77*, 1262–1265. https://doi.org/10.1103/physrevlett.77.1262

Aurell, E., Boffetta, G., Crisanti, A., Paladin, G., & Vulpiani, A. (1997). Predictability in the large: An extension of the concept of Lyapunov exponent. *Journal of Physics*, *A30*, 1–26. https://doi.org/10.1088/0305-4470/30/1/003

Boffetta, G., Giuliani, P., Paladin, G., & Vulpiani, A. (1998). An extension of the Lyapunov analysis for the predictability problem. *Journal of the Atmospheric Sciences*, *55*, 3409–3416. https://doi.org/10.1175/1520-0469(1998)055<3409:aeotla>2.0.co;2

DelSole, T. (2004). Predictability and information theory. Part I: Measures of predictability. *Journal of the Atmospheric Sciences*, *61*, 2425–2440. https://doi.org/10.1175/1520-0469(2004)061<2425:paitpi>2.0.co;2

DelSole, T., & Tippett, M. K. (2007). Predictability: Recent insights from information theory. *Reviews of Geophysics*, *45*, RG4002. https://doi.org/10.1029/2006RG000202

Durran, D. R., Reinecke, P. A., & Doyle, J. D. (2013). Large-scale errors and mesoscale predictability in Pacific northwest snowstorms. *Journal of the Atmospheric Sciences*, *70*, 1470–1487. https://doi.org/10.1175/jas-d-12-0202.1

Emanuel, K. A., & Zhang, F. (2016). On the predictability and error sources of tropical cyclone intensity forecasts. *Journal of the Atmospheric Sciences*, *73*, 3739–3747. https://doi.org/10.1175/JAS-D-16-0100.1

Goldhirsch, I., Sulem, P. L., & Orszag, S. A. (1987). Stability and Lyapunov stability of dynamical systems: A differential approach and a numerical method. *Physica*, *27D*, 311–337. https://doi.org/10.1016/0167-2789(87)90034-0

Hakim, G. J. (2011). The mean state of axisymmetric hurricanes in statistical equilibrium. *Journal of the Atmospheric Sciences*, *68*, 1364–1376. https://doi.org/10.1175/2010jas3644.1

Hakim, G. J. (2013). The variability and predictability of axisymmetric hurricanes in statistical equilibrium. *Journal of the Atmospheric Sciences*, *70*, 993–1005. https://doi.org/10.1175/jas-d-12-0188.1

Jordan, C. L. (1958). Mean soundings for the West Indies area. *Journal of Meteorology*, *15*, 91–97. https://doi.org/10.1175/1520-0469(1958)015<0091:msftwi>2.0.co;2

Judt, F. (2018). Insights into atmospheric predictability through global convection-permitting model simulations. *Journal of the Atmospheric Sciences*, *75*(5), 1477–1497. https://doi.org/10.1175/jas-d-17-0343.1

Judt, F., Chen, S. S., & Berner, J. (2015). Predictability of tropical cyclone intensity: Scale-dependent forecast error growth in high-resolution stochastic kinetic-energy backscatter ensembles. *Quarterly Journal of the Royal Meteorological Society*, *142*(694), 43–57. https://doi.org/10.1002/qj.2626

Kieu, C. (2015). Hurricane maximum potential intensity equilibrium. *Quarterly Journal of the Royal Meteorological Society*, *141*, 2471–2480. https://doi.org/10.1002/qj.2556

Kieu, C. Q., Keshavamurthy, K., Tallapragada, V., Gopalakrishnan, S., & Trahan, S. (2018). On the growth of intensity forecast errors in the operational hurricane weather research and forecasting (HWRF) model. *The Quarterly Journal of the Royal Meteorological Society*, *144*, 1803–1819. https://doi.org/10.1002/qj.3344

Kieu, C. Q., & Moon, Z. (2016). Hurricane intensity predictability. *Bulletin of the American Meteorological Society*, *97*(10), 1847–1857. https://doi.org/10.1175/bams-d-15-00168.1

Kieu, C. Q., & Wang, Q. (2017). Stability of tropical cyclone intensity equilibrium. *Journal of the Atmospheric Sciences*, *74*, 3591–3608. https://doi.org/10.1175/jas-d-17-0028.1

Kraichnan, R. H. (1967). Inertial ranges in two-dimensional turbulence. *Physics of Fluids*, *10*, 1417–1423. https://doi.org/10.1063/1.1762301

Leith, C. E. (1971). Atmospheric predictability and two-dimensional turbulence. *Journal of the Atmospheric Sciences*, *28*, 145–161. https://doi.org/10.1175/1520-0469(1971)028<0145:apatdt>2.0.co;2

Leith, C. E., & Kraichnan, R. H. (1972). Predictability of turbulent flows. *Journal of the Atmospheric Sciences*, *29*, 1041–1058. https://doi.org/10.1175/1520-0469(1972)029<1041:potf>2.0.co;2

Lorenz, E. N. (1963). Deterministic nonperiodic flow. *Journal of the Atmospheric Sciences*, *20*, 130–141. https://doi.org/10.1175/1520-0469(1963)020<0130:dnf>2.0.co;2

Lorenz, E. N. (1969). The predictability of a flow which possesses many scales of motion. *Tellus*, *21*, 289–307. https://doi.org/10.3402/tellusa.v21i3.10086

Mathieu, J. (2000). *An introduction to turbulent flow* (1st ed., p. 374). Cambridge University Press.

Métais, O., & Lesieur, M. (1986). Statistical predictability of decaying turbulence. *Journal of the Atmospheric Sciences*, *43*, 857–870.

Palmer, T. N. (1993). Extended-range atmospheric prediction and the Lorenz model. *Bulletin of the American Meteorological Society*, *74*, 49–65. https://doi.org/10.1175/1520-0477(1993)074<0049:erapat>2.0.co;2

Palmer, T. N., Doring, A., & Seregin, G. (2014). The real butterfly effect. *Nonlinearity*, *27*, 123–141. https://doi.org/10.1088/0951-7715/27/9/r123

Piessens, R. (2010). *The transforms and applications handbook* (3rd ed.). CRC Press.

Rotunno, R., & Emanuel, K. A. (1987). An air–sea interaction theory for tropical cyclones. Part II: Evolutionary study using a non-hydrostatic axisymmetric numerical model. *Journal of the Atmospheric Sciences*, *44*, 542–561. https://doi.org/10.1175/1520-0469(1987)044<0542:aaitft>2.0.co;2

Rotunno, R., & Snyder, C. (2007). A generalization of Lorenz's model for the predictability of flows with many scales of motion. *Journal of the Atmospheric Sciences*, *65*, 1063–1076.

Schneider, T., & Griffies, S. (1999). A conceptual framework for predictability studies. *Journal of Climate*, *12*, 3133–3155. https://doi.org/10.1175/1520-0442(1999)012<3133:acffps>2.0.co;2

Schubert, W. H., Rozoff, C. M., Vigh, J. L., McNoldy, B. D., & Kossin, J. P. (2007). On the distribution of subsidence in the hurricane eye. *Quarterly Journal of the Royal Meteorological Society*, *133*, 595–605. https://doi.org/10.1002/qj.49

Shukla, J. (1981). Dynamical predictability of monthly means. *Journal of the Atmospheric Sciences*, *38*, 2547–2572. https://doi.org/10.1175/1520-0469(1981)038<2547:dpomm>2.0.co;2

Tribbia, J. J., & Baumhefner, D. P. (2004). Scale interactions and atmospheric predictability: An updated perspective. *Monthly Weather Review*, *132*, 703–713. https://doi.org/10.1175/1520-0493(2004)132<0703:siaapa>2.0.co;2

Vallis, G. K. (2017). *Atmospheric and Oceanic fluid dynamics* (p. 946). Cambridge University Press.

Vonich, P. T., & Hakim, G. J. (2018). Hurricane kinetic energy spectra from in situ aircraft observations. *Journal of the Atmospheric Sciences*, *75*, 2523–2532. https://doi.org/10.1175/jas-d-17-0270.1

Worsnop, R. P., Bryan, G. H., Lundquist, J. K., & Zhang, J. A. (2017). Using large-eddy simulations to define spectral and coherence characteristics of the hurricane boundary layer for wind-energy applications. *Boundary-Layer Meteorology*, *165*, 55–86. https://doi.org/10.1007/s10546-017-0266-x

Yang, B., Wang, Y., & Wang, B. (2007). The effect of internally generated inner-core asymmetries on tropical cyclone potential intensity. *Journal of the Atmospheric Sciences*, *64*, 1165–1188. https://doi.org/10.1175/jas3971.1

Yu, Z., Wang, Y., & Xu, H. (2015). Observed rainfall asymmetry in tropical cyclones making landfall over China. *Journal of Applied Meteorology and Climatology*, *54*, 117–136. https://doi.org/10.1175/jamc-d-13-0359.1

Zhang, D.-L., & Kieu, C. Q. (2005). Shear-forced vertical circulations in tropical cyclones. *Geophysical Research Letters*, *32*, L13822. https://doi.org/10.1029/2005GL023146